Curvature effect on the surface diffusion of silver adatoms on carbon nanotubes: Deposition experiments and numerical simulations

Ming-Chya Wu,[1,*] Cui-Lian Li,[1,2] Chin-Kun Hu,[1,†] Yuan-Chih Chang,[1] Yuan-Hong Liaw,[1] Li-Wei Huang,[1] Chia-Seng Chang,[1,‡] Tien-Tzou Tsong,[1] and Tung Hsu[3]

[1]*Institute of Physics, Academia Sinica, Nankang, Taipei 11529, Taiwan*

[2]*Department of Physics, Shanghai Jiao Tong University, Shanghai 200030, China*

[3]*Department of Materials Science and Engineering, National Tsing-Hua University, Hsinchu 30013, Taiwan*

(Received 5 May 2006; revised manuscript received 11 August 2006; published 27 September 2006)

The cluster formation of silver adatoms on carbon nanotubes (CNTs) is investigated to infer the curvature effect on surface diffusion. By analyzing the cluster density as a function of the deposition time t for different diameters d_c of CNTs, we obtain the scaling form for describing the curvature effect on surface diffusion in the first-order approximation. We find that the curvature effect on the surface diffusion can well be described by using the relation between the deposition time t and the scaled deposition time τ in the form of $\tau \sim t d_c^{-z}$, with z being the exponent characterizing geometric properties of CNTs and the nanotube helicity. The value of z for the armchair-type CNT is larger than those for the zig-zag type and the chiral-type CNTs. The scaling form is further demonstrated and verified by numerical simulations, and is explained by the two-dimensional random walk model. Our study may provide a potential application of determining the armchair-type single-wall CNT from measuring the value of z.

DOI: 10.1103/PhysRevB.74.125424 PACS number(s): 73.22.−f, 68.43.De, 68.43.Jk

I. INTRODUCTION

Surface diffusion of adatoms plays an important role in the microscopic mechanism of many surface processes,[1–3] such as adsorption and desorption, surface reaction, and crystal growth. Recently, the study of the growth of metallic atoms on carbon nanotubes (CNTs)[4] has attracted considerable attention. One reason is its importance for the physics in nanoscale, and the other is the possibility for the implementation of microdevices by CNTs. For the latter, deposition of metallic atoms on CNTs has been a practical technique widely used to design particular functions for certain purposes. For example, nanoleads can be fabricated by depositing metallic atoms on the surface of CNTs with well-controlled adsorption and migration processes.[5] Adatom diffusion is obviously of fundamental importance for such systems.

The study of adatom diffusion on the surface of a CNT involves the theory for interactions between adatom and carbon (C) atoms in the CNT, and requires the knowledge of quantum physics and chemistry in atomic scale. However, it can be simplified to classical level, provided that the system is considered as simple motions of particles in an effective potential established by the C atoms in the CNT. Due to bond deformation, the curved surface of a CNT has properties which are different from those of a flat, strain-free surface.[6] It is thus expected to lead to adatom diffusion processes different from those of an adatom on a flat surface. Recently, the importance of curvature effects on adsorption and migration of adatoms has been addressed and emphasized.[6,7] However, little is known about how metallic atoms adsorb and migrate over the surface of a CNT. As a result, even though it is proposed that the curvature effect appears to be important for adsorption and migration, there is still no empirical evidence supporting the proposal.

In this paper, we report the curvature effect on the surface diffusion of silver (Ag) adatoms on CNTs from experimental and theoretical aspects. Based on the scaling analysis of empirical data, we assume a scaling form for describing the curvature effect on surface diffusion. The scaling form is parameterized by two constants to be determined from experiments. We then determine the parameters from fitting empirical data and use them to demonstrate the cluster formation of adatoms by numerical simulations to verify our assumptions. The simulation results confirm that the scaling form can well describe the curvature effect on the surface diffusion of Ag atoms on CNTs. Furthermore, to have theoretical explanations on the scaling form, a simple derivation of the scaling form is further provided by considering the anisotropic two-dimensional random walk model. The model heuristically explains the range of the scaling exponent in the scaling form.

The paper is organized as follows. In Sec. II, we introduce the experimental setup for performing the cluster formation of Ag atoms on CNTs and present the experimental results. The scaling analyses are discussed in detail in Sec. III, and the numerical simulations are performed in Sec. IV. In Sec. V, we further derive the scaling form by using the two-dimensional random walk model. Finally, we conclude our results in Sec. VI.

II. EXPERIMENTS

In our experimental setup, Ag atoms from an electron-beam evaporator are deposited onto the CNTs. An ultrahigh-vacuum transmission electron microscope (UHV TEM, JEOL JEM-2000V) is employed to *in situ* record the formation and growth of the Ag clusters. The base pressure of the microscope is 2×10^{-10} Torr and is under 6×10^{-10} Torr during the Ag deposition. The CNT samples are suspended in isopropyl alcohol and then dropped on the perforated C film supported by the copper grid. The sample can be quickly exchanged through a load-lock chamber gated with a valve

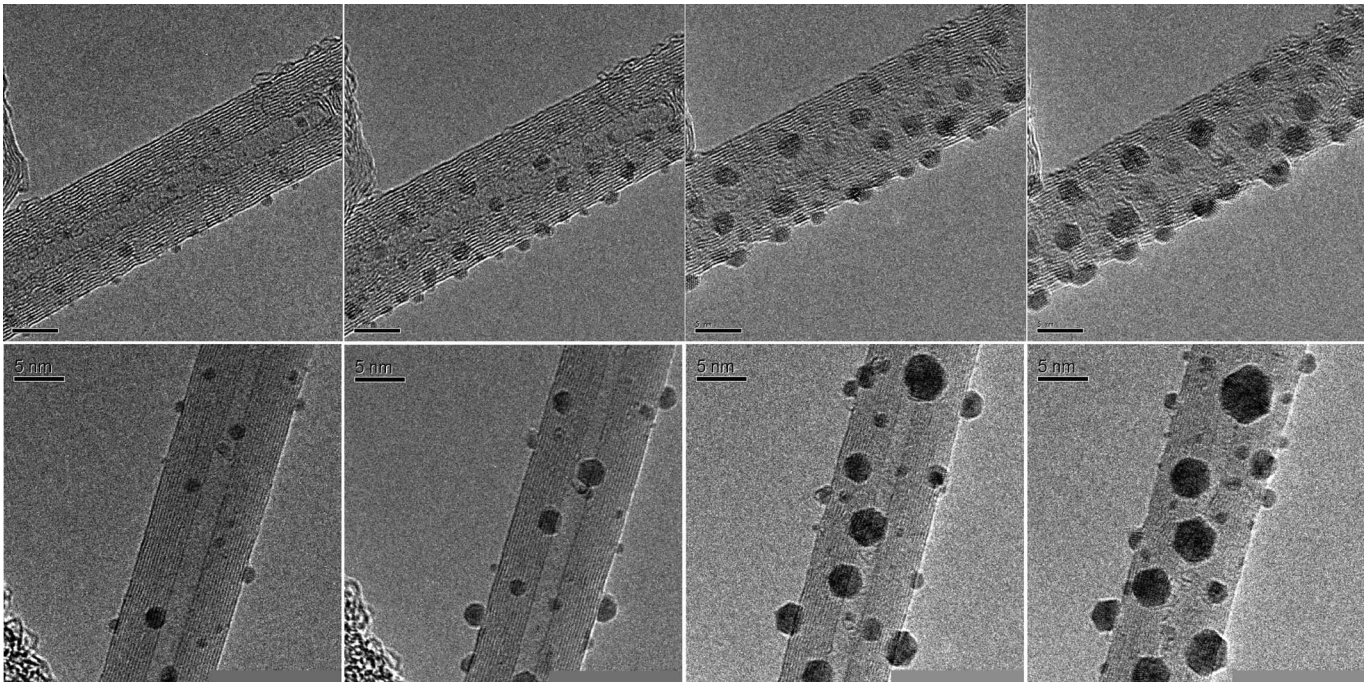

FIG. 1. Sequential TEM images of the formation of Ag clusters on the CNTs at two different temperatures. Images in the top row were taken at room temperature 296 K (heating current I_h=0) and those in the bottom at 503 K (I_h=0.17 A). From the left frame to right, the images were taken with time at about 5, 15, 35, and 55 min after Ag deposition. The scale bars are 5 nm in length.

to the main chamber of the TEM. A charge-coupled device (CCD) camera with one million pixels is operated at one frame per second to capture the dynamic behavior of the adsorbed Ag atoms and clusters. The CNTs can be heated by passing an electric current through a metal coil installed in the sample holder. The temperature of the corresponding heating current is measured by a thermal couple at the sample stage. However, the true temperature at the place where the image is taken is likely higher due to the electron-beam irradiation. Figure 1 shows typical sequential TEM images of the formation of Ag clusters on the CNTs at two different temperatures.

To describe the behaviors of the cluster formation of Ag adatoms, we define the cluster density η as

$$\eta = \frac{N}{\pi d_c l}, \tag{1}$$

where N is the number of clusters on the surface of the CNT with diameter d_c and length[8] l in the unit of nanometer (nm). The cluster density η is a function of the deposition time t, the curvature (R) of a CNT,[7] and the diffusion rate (ρ) of Ag adatoms. Here, the diffusion rate ρ is related to the temperature of adatoms heated by the electric current I_h. Furthermore, the curvature R is defined by[6]

$$R = \frac{\sigma}{d_c}, \tag{2}$$

where σ is a parameter describing the radius of the interaction between the adatom and the C atoms in the CNT. Thus, the curvature R explicitly enters into the function of η via d_c.

The specifications of the CNTs and experimental settings used in the experiments, and the corresponding derivatives, are listed in Table I. The relation between I_h and T is roughly linear and can be described by $T=296+1217I_h$. The experimental results for the cluster density as a function of the deposition time are shown in Fig. 2. The curves of Fig. 2(a) illustrate the cluster density η as a function of t for different d_c, and those shown in Fig. 2(b) illustrate the same but are for different d_c, and I_h. In Fig. 2(a), there are two groups, one with a shorter deposition time ($t<30$ min) and the other with a longer deposition time ($t>50$ min). The curve of graphite is included for comparison. All the curves in Fig. 2(b) were recorded for $t>50$ min with the CNTs heated by the specified current.

III. SCALING ANALYSIS FOR THE CURVATURE EFFECT

According to the behaviors of η shown in Figs. 2(a) and 2(b), we propose that η can be written as $\eta=\eta(t,R,\rho)$. The cluster density η saturates at η_s after a characteristic threshold of the deposition time $t_s(R,\rho)$. The curves shown in Figs. 2(a) and 2(b) can be generally described by three stages. In the first stage with $t<t_s$, Ag atoms fall on the surface of a CNT and diffuse in a limited degree of freedom defined by the structure of CNT.[6] As two or more Ag adatoms move to be the nearest neighbors, they form a cluster and immobilize when the cluster is large enough. Therefore, the number of clusters increases with time before $t<t_s$. This stage is known as *nucleation*. In the second stage known as *growth*, the cluster density saturates, and the nucleation and combination enter into the equilibrium state, i.e., the number of clusters is roughly kept constant in average, and the cluster size grows.

TABLE I. Specifications of the CNTs and settings used in the experiments, where d_c is the diameter of CNT, l is the length, n is the number of layers of C atoms, ζ is the aspect ratio defined as $\zeta=\pi d_c/l$, R is the curvature, I_h is the electric current for heating, T is the temperature, and z is the exponent defined in Eq. (6).

d_c (nm)	l (nm)	n	ζ	R/σ	I_h (A)	T (K)	z
3.46	21.39	4	0.508	0.289	0	296	0.50
4.28	20.21	4	0.665	0.234	0	296	0.50
5.45	30.50	7	0.561	0.183	0	296	0.75
10.40	26.72	13	1.223	0.096	0	296	0.50
13.13	25.47	20	1.620	0.076	0	296	0.50
16.25	14.05	22	3.634	0.062	0	296	0.50
8.13	16.58	10	1.540	0.123	0.10	413	0.75
9.25	22.04	12	1.318	0.108	0.15	478	0.75
10.30	16.72	12	1.935	0.097	0.07	383	0.50
10.40	15.21	14	2.148	0.096	0.17	503	1.00
11.16	17.43	16	2.011	0.090	0.12	443	0.50

The third stage known as *ripening* starts when η starts to decline gently. In this stage, the average cluster sizes reach a critical value, and the effect of combination of two or more clusters into a larger cluster dominates.

Recently, theoretical studies showed that curvatures and helicities (chiralities) significantly affect the diffusion of adatoms on the surfaces of CNTs.[6] The general picture is that positive curvature increases the diffusion barrier and corrugates the potential energy surface. Theoretical calculations show that the migration barriers of Ag atoms on CNTs is 0.2–0.3 eV.[9] The helicity also plays an important role on the diffusion path, and different types of CNTs have different diffusion paths.[6] To understand the roles the curvature effect and helicity play in our empirical observations, here we use the scaling analysis. The analysis relies on the assumption that if the curvature effects can be described by scaling in a proper way, the curves in Fig. 2 will roughly collapse into a single curve when we plot scaled η as a function of a scaled deposition time τ. For this purpose, we take η/η_s as scaled η and use the geometric property of CNTs to define τ and have

$$\bar{\eta} \equiv \frac{\eta(t,R,\rho)}{\eta_s} = \bar{\eta}(\tau,\rho). \tag{3}$$

It has been well known that structures of CNTs can be classified into the zig-zag, armchair, and chiral forms, as shown in Figs. 3(a)–3(c), respectively. There is still a lack of

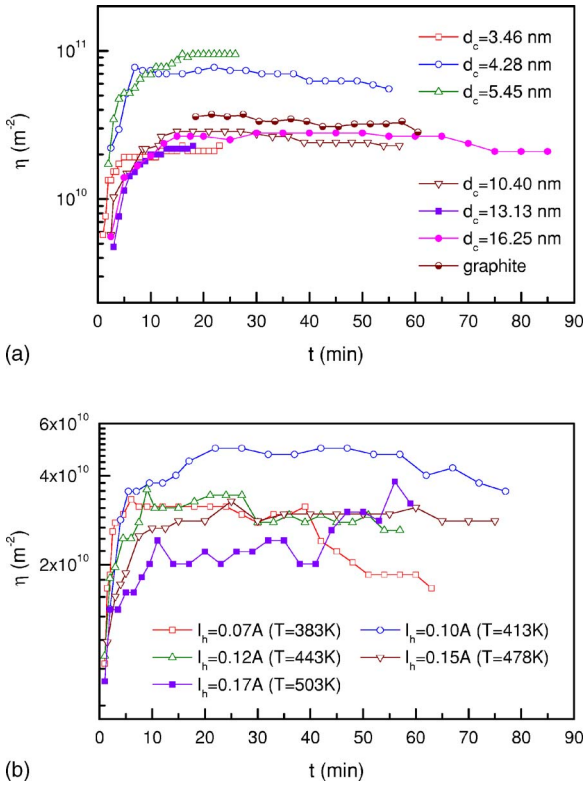

FIG. 2. (Color online) Cluster density η as a function of t for (a) different d_c and $I_h=0$, and (b) different d_c and $I_h\neq 0$. The curve of graphite shown in (a) is for comparison.

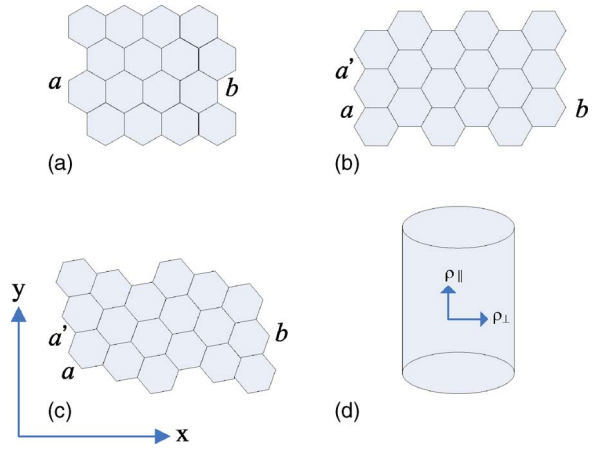

FIG. 3. (Color online) Schematic drawing for typical honeycomb structures of (a) the zig-zag type (a connects to b), (b) the armchair-type (a connects to b), and (c) the chiral-type (a' connects to b) CNTs. (d) The relation between components of the diffusion rate and the orientation of the CNT.

control over the helicities at the growth stage of CNTs, and there is no practical approach available for determining the helicity γ of a multiwall CNT. We thus do not know the helicities of the CNTs used in our experiments.

Since $\bar{\eta}$ depends on the diffusion rate ρ, we first analyze the dependence of ρ on geometry of CNTs, represented by R and γ, and applied current I_h. We take a vector form of diffusion rate

$$\vec{\rho}(\gamma,R,I_h) = \rho_\perp(\gamma,R,I_h)\hat{\theta} + \rho_\parallel(\gamma,R,I_h)\hat{j}, \tag{4}$$

where the coordinate is defined according to the orientation of a CNT [along the y direction, as shown in Fig. 3(d)], such that $\hat{\theta}$ and $\hat{j}$ are unit vectors of the azimuthal angle and axial component, respectively. The ratio between $\rho_\perp$ and $\rho_\parallel$ in Eq. (4) is generally determined by the structure of the CNT. According to studies of Shu and Gong,[6] $\rho_\parallel$ is zero for the armchair-type CNT if the thermal energy of the adatom is lower than the axial energy barrier. For the case of the zig-zag type CNT, the ratio between $\rho_\perp$ and $\rho_\parallel$ is nonzero and of the order of unity. Since the curvature effect enhances the energy barrier,[6] the dependence of ρ on R is stronger in the armchair-type CNT than in the zig-zag type CNT.

As the current I_h is applied to the system, the temperature T of the system is increased and the diffusion rate ρ also increases. We find that the relation between T and I_h in our system is roughly linear within the temperature range of experiments. Hence, we assume a linear relation[10] between the increment of diffusion rate $(\Delta\rho)$ and I_h, i.e.,

$$\Delta\rho \propto I_h. \tag{5}$$

In critical lattice systems,[11] the linear dimension of the system has been used to define the scaling variable.[12–15] Since the lengths of CNTs are usually ambiguous,[8] the most relevant linear dimension of a CNT is its diameter d_c. Under the condition of constant flux of Ag atoms falling on the surfaces of CNTs in the experiments and Eq. (5), Eq. (4) can be explicitly expressed as

$$\vec{\rho}(\gamma,R,I_h) = \rho_0(1+F_1I_h)[d_c^{-z}\hat{\theta} + \alpha(\gamma)\hat{j}], \tag{6}$$

where ρ_0 and F_1 are constants, z is the exponent for the dependence of the diffusion on d_c, and $\alpha=0$ for the armchair-type CNT and $\alpha\neq 0$ for the zig-zag and chiral-type CNTs. Wang and Hu[13] had defined the scaling variable for the dynamic lattice Ising model as tL^{-z}, where t is time, L is the linear dimension of the lattice, and z is the dynamic critical exponent.[16] Thus, Eq. (6) suggests that we can define the scaled deposition time τ as

$$\tau = F_2(1+F_1I_h)td_c^{-z}. \tag{7}$$

Here F_2 is a constant related to ρ_0 and the flux of Ag atoms and can be set to be 1. Consequently, there is only one parameter (z) to be determined in the case of $I_h=0$, and two parameters (F_1 and z) in the case of $I_h\neq 0$. According to the experimental data, the order of F_1 should be taken as $O(0.01)$ to have the best scaling. Accordingly, in the following, we will take $F_1=0.01$. Equation (7) implies that the threshold of the deposition time $t_s(R,\rho)$ can be written as

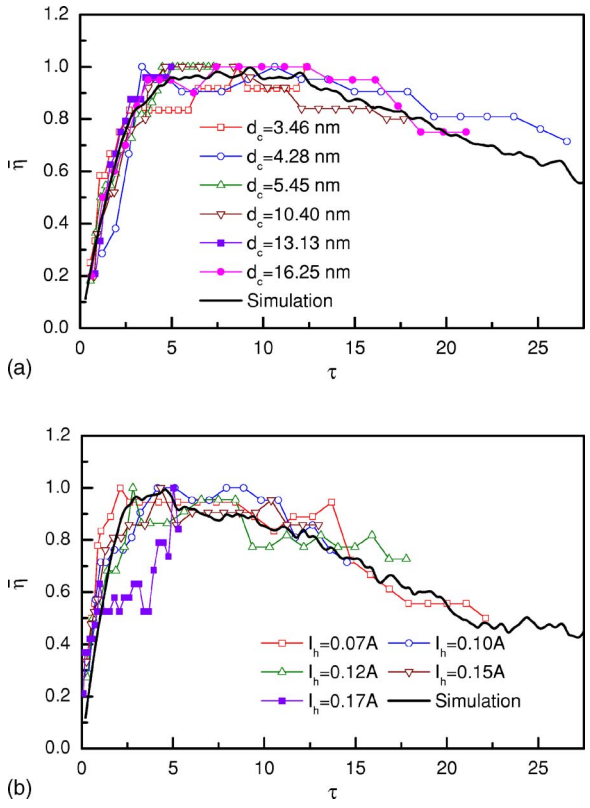

FIG. 4. (Color online) The normalized cluster density $\bar{\eta}$ as (a) a function of τ and d_c, and (b) a function of τ, d_c, and I_h.

$$t_s(R,\rho) \propto (1+F_1I_h)^{-1}d_c^z\tau_s(R,\rho). \tag{8}$$

The normalized cluster density $\bar{\eta}$ as a function of τ for different d_c are shown in Fig. 4(a), and the values of z used are listed in Table I. The CNT with the diameter of d_c $=5.45$ nm has a distinct z of 0.75 and is likely an armchair-type CNT, which will be discussed further below. The results of Fig. 4(a) are impressive since all data roughly collapse into a curve. Because the realizations in Fig. 4(a) are non-self-averaging, the small deviations can be considered as being originated from different types (structures) of CNTs. For example, different helicities lead to different diffusion paths, which in turn set different restrictions to cluster formations. This feature will be examined later by numerical simulations. The common behavior for the curves in Fig. 4(a) is that the normalized cluster density, $\bar{\eta}$, starts from zero at $\tau=0$ to the saturated density, $\bar{\eta}=1$, at $\tau\approx 5$. The saturation extends from $\tau\approx 5$ to $\tau\approx 10$, and then $\bar{\eta}$ starts to decline gently. The single curve for different d_c in Fig. 4(a) implies the curvature effect can be substantially described by the relations formulated in Eqs. (6) and (7).

We further apply the scaling analysis to the case of I_h $\neq 0$, and the results are shown in Fig. 4(b). The values of z for different realizations are listed in Table I. The larger value of z for $I_h\neq 0$ implies a smaller ratio of $\rho_\parallel/\rho_\perp$ at higher temperatures. This could be due to the effect that higher temperature anisotropically enhances the surface diffusion. As a result, the curvature effect may be further overestimated and the value of z becomes larger. This implies Eqs. (6) and (7) with $z\simeq\frac{1}{2}$ are applicable only for the case with small I_h.

Further, we find that $\bar{\eta}$ for small I_h (<0.15 A) generally follows a similar path with significant fluctuations in comparison with those with zero I_h. However, the trend of $\bar{\eta}$ for large I_h (>0.15 A) can be very different from those with small and zero I_h. This indicates that there is a critical electric current (temperature) for the surface diffusion. When an electric current exceeding the critical value is applied, the adsorption becomes loose such that a cluster can continue to move even with a large cluster size (see the bottom images of Fig. 1), and the diffusion path becomes more free. This effect finally leads to an unusually large (overestimated) value of $z(=1)$. Here we should note that the realizations with zero and nonzero I_h were regarded as different groups, and the time scale in Fig. 4(b) has been rescaled with different parameters from that in Fig. 4(a). Thus the profiles in Figs. 4(a) and 4(b) can be different.

IV. NUMERICAL SIMULATIONS

Next, we simulate the cluster formations on CNTs based on the assumptions that the adsorption is uniform, and adsorbed atoms can diffuse freely in specified directions before forming clusters. To take the structures of CNTs into account, we consider the diffusion direction and diffusion rate as control parameters and take the periodic boundary conditions in the $\hat{\theta}$ direction. In short, the cluster formation is described by the following model. We first take the diameter r_0 of an Ag atom (about 2 Å) as a basic unit and set $r_0=1$; thus, 1 nm allows 5 Ag atoms in a row. The surface of a CNT is mapped to a planar lattice with size $5\pi d_c \times 5l$ to make the lattice size in simulation consistent with real CNTs. The process of the constant flux of Ag atoms randomly falling on the plane is simulated by the constant rate (number per unit time) of Ag atoms being generated on the surface.

According to the theoretical studies of Krasheninnikov *et al.*[7] and Durgun *et al.*,[9] the most favorable binding site for adatoms depends on the adatom and the type of CNTs. However, there is as yet no experimental evidence for the favorable binding sites of Ag atoms on CNTs.[17] In the case that an Ag adatom favorably locates at the center of the honeycomb lattice, the "sites" which Ag atoms adsorb form a triangular lattice. On the other hand, if an adatom will locate at one of the middle of the six honeycomb bridges, then the sites form a honeycomb lattice. In the latter case, the radius of the Ag atom excludes the possibility of two Ag atoms locating at adjacent bridges. As one Ag atom adsorbs at one bridge, the nearest four bridges cannot be occupied by other atoms. Therefore, an additional rule for the diffusion path should be imposed in this case for each adatom to check the next site where it can move. This leads to a complicated situation for various possibilities. In order to catch essential features of the cluster formation, here we will simply consider deposition and diffusion of Ag atoms on a square lattice.

In our simulation, the deposition time t is proportional to the number of steps in the algorithm. Thus, we control both the falling rate of Ag atoms and the diffusion rate of Ag adatoms. The simulation consists of two steps:

1. At time t_i, n_a Ag adatoms are generated and distributed randomly on the lattice.

2. At time t_{i+1}, an adatom can diffuse in four directions with equal probability in the zig-zag type CNT, with nonequal probability in the chiral-type CNT, and can only diffuse along the circumference with equal probability in the armchair-type CNT. The diffusion rate in the simulation should follow Eq. (6) to take into account the curvature effect which appears as d_c^{-z} in $\vec{\rho}$. When two adatoms (or one adatom and one cluster) with radii r_1 and r_2, respectively, contact within a distance smaller than (r_1+r_2) or overlap, they coalesce with mass conservation to form a cluster (or merge with a larger cluster) with a radius $r=(r_1^d+r_2^d)^{1/d}$, with d being the effective dimension of the cluster.[18] Later, the cluster will be regarded as a new individual in the next simulation step. All adatoms update once in this step. This step repeats m times until time t_{i+m}.

At time t_{i+m+1}, step 1 is repeated and n_a Ag adatoms are generated again on the lattice and the simulation repeats step 2. Such processes are iterated until the required number of iterations is reached.

The effective dimension d is generally compared with the spacial dimension D. When $d \leqslant D$, we have $r \geqslant (r_1^D+r_2^D)^{1/D}$, and a single cluster forms and extends across the entire system in a finite time. This situation is similar to percolation and gelation phenomena. For the case of $d>D$, we have $r<(r_1^D+r_2^D)^{1/D}$ and there is no gelation in a finite time and the growth proceeds much in the same manner as in low-density colloidal aggregation. Since the experimental condition under consideration corresponds to $d=3$ and $D=2$, our simulation should exhibit a scenario similar to the case of $d>D$.

The number of clusters is monitored at each time step. Finally, we get the number of clusters as a function of the simulation time. By adjusting these control parameters for the case of $I_h=0$, the curve of a typical realization obtained from simulations can fit experimental results well, as shown in Fig. 4(a). The falling rate (n_a/m) used in the simulation is four atoms $(n_a=4)$ per hundred simulation steps $(m=100)$, the system size is 86×153 (roughly in the scale of $5\pi d_c \times 5l$), $\rho_0=10$, $\alpha=1$, and $d_c=5.45$ are taken, and a cluster with two Ag atoms cannot move. The value of $F_2=\frac{2}{3}$ is used in Eq. (7) to correct the selected value of ρ_0 to have a better fitting. Similarly, we can simulate a realization with $F_1=0.01$ to fit the cases with nonzero I_h, and the results are shown in Fig. 4(b).

To demonstrate our model quantitatively, we further simulate realizations by Eq. (6) with predetermined parameters for different d_c and l which are compatible with the specifications of the CNTs used in experiments (but $z=\frac{1}{2}$ is assumed for all realizations), and the results are shown in Fig. 5(a). Similarly, we simulate the situations with nonzero I_h and $F_1=0.01$, and the results are shown in Fig. 5(b). The significant agreement between experimental results and simulations implies that the picture we proposed catches the essential factors in the cluster formation of Ag adatoms on CNTs.

As mentioned above, the value of z also characterizes the geometric properties (e.g., helicity) of CNTs. In order to have more insight into the effect of helicity and to verify the scaling form of Eq. (7), we further keep $|\vec{\rho}| \simeq 10$ and take different values of $\rho' = \rho_\parallel / \rho_\perp$ in Eq. (4) for the simulations of

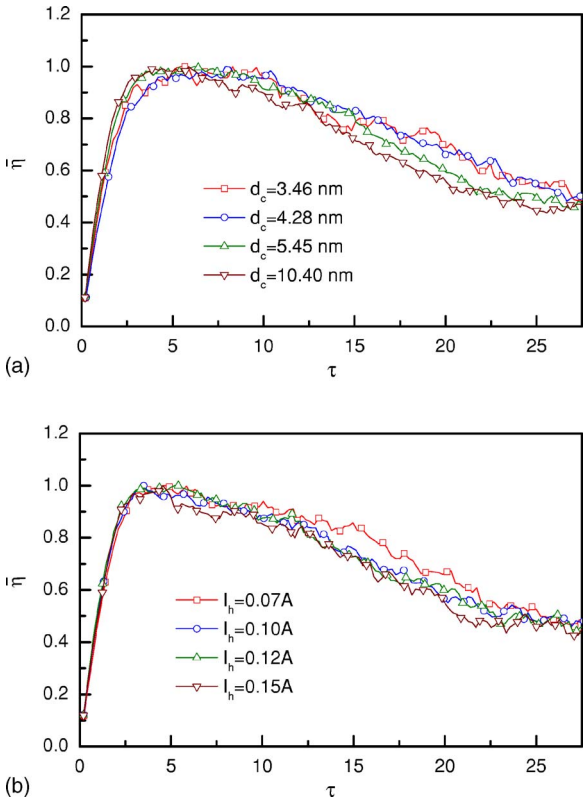

FIG. 5. (Color online) Simulations for (a) $I_h=0$ and (b) $I_h\neq 0$. The same specifications of the CNTs as those in experiments (see Table I) and $z=0.5$ have been used in these simulations.

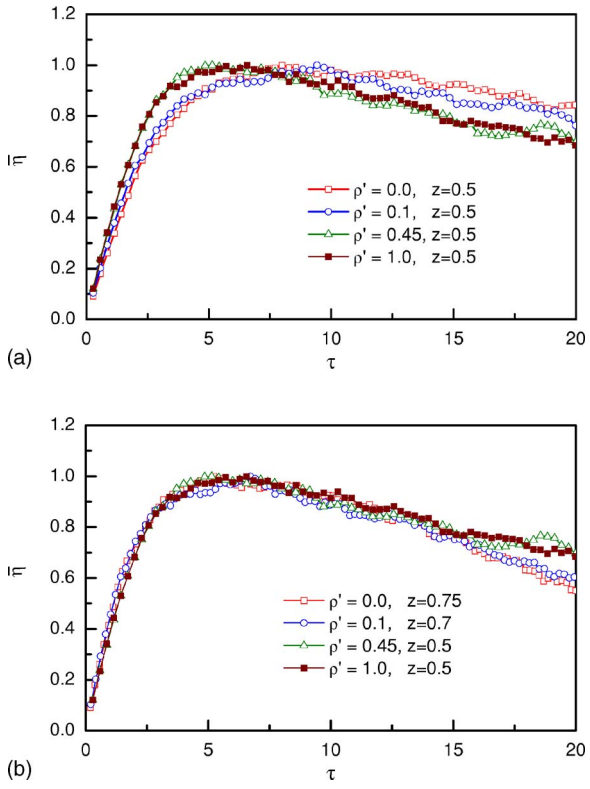

FIG. 6. (Color online) Simulations for different $\rho'=\rho_\parallel/\rho_\perp$ ratios, and τ is rescaled with (a) $z=0.5$ for all ρ', and (b) $z=0.75$ for $\rho'=0$, $z=0.7$ for $\rho'=0.1$, $z=0.5$ for $\rho'=0.45$, and $z=0.5$ for $\rho'=1.0$.

the cases with $I_h=0$. From our analysis, different values of ρ' correspond to different types of CNTs. For instance, $\rho'=0$ corresponds to the armchair-type CNT. Thus, simulations using Eq. (4) with different ρ' in simulations resemble real experiments for different types of CNTs. Except for using Eq. (4) instead of Eq. (6), we use the same simulation algorithm disclosed above. The parameters used here are also the constant falling rate of four atoms per area per 100 simulation steps on a lattice with size 86×153, and $(\rho_\perp,\rho_\parallel)=(10,0),(10,1),(9,4),(7,7)$ for $\rho'=0,0.1,0.45,1$. More specifically, an Ag atom can either move $\rho_\perp$ sites in $\pm\hat{\theta}$ directions or $\rho_\parallel$ sites in $\pm\hat{j}$ directions with a probability generated by computers in one simulation step. Note that under the conditions of constant falling rate of Ag atoms and $\rho_\parallel$ and $\rho_\perp$ being smaller than the lattice size, the choice of other lattice sizes does not alter the results. We first use $z=\frac{1}{2}$ in τ for all ρ' in the scaling analysis, and the results are shown in Fig. 6(a). The deviations of four curves in the range of $\tau<10$ demonstrate the effects of $\rho_\parallel/\rho_\perp$ originated from the nanotube helicity. According to the scaling analysis presented above, we can take different values of z for different ρ' to compensate these effects. We then adjust the values of z in τ to make the four curves collapse, and the results are shown in Fig. 6(b). The remarkable coincidence of the four curves indicates the effect of $\rho_\parallel/\rho_\perp$, which plays a crucial role during the nucleation and growth stages in the case of $I_h=0$, can well be described by the exponent z. It follows that the scaling form in Eq. (7) is verified. Furthermore, the curve with $\rho'=0$ is rescaled with the largest value of z. Since $\rho'=0$ corresponds to the armchair-type CNT, this implies that from comparing the value of z the armchair-type CNT is distinguishable from the zig-zag and chiral-type CNTs. This provides a potential application of this study that one can determine the armchair-type CNT from measuring the value of z.

V. RANDOM WALK ANALYSIS

In light of the simulations in Sec. IV, a simple derivation for the exponent z is available from considering the anisotropic two-dimensional random walk model.[19] Since the curvature effect and nanotube helicity can be considered as anisotropic controls on the diffusion rate, we assume the step lengths are $\rho_\parallel$ in the $\pm\hat{j}$ directions and $\rho_\perp$ in the $\pm\hat{\theta}$ directions in the random walk. After t steps, we get a sum of t two-dimensional vectors with random orientations in a plane. The average of the final position r after t steps is[20]

$$\langle |r|^2\rangle = t\sqrt{\rho_\perp^2+\rho_\parallel^2}. \tag{9}$$

The root-mean-square distance after t steps is thus

$$|r|_{\rm rms} = t^{1/2}(\rho_\perp^2+\rho_\parallel^2)^{1/4}. \tag{10}$$

The scaling analysis essentially corresponds to the consideration of a walk with unit step length. Therefore, we compare Eq. (10) and that for the isotropic case with the unit step length $\bar{\rho}$ ($\approx\sqrt{\rho_\perp^2+\rho_\parallel^2}$ is assumed here) and τ steps. The con-

dition for two walks to reach the same position r is

$$\tau\bar{\rho} \sim t(\rho_\perp^2 + \rho_\parallel^2)^{1/2}. \tag{11}$$

Thus we have

$$\tau \sim t\left(\frac{\rho_\perp^2 + \rho_\parallel^2}{\bar{\rho}^2}\right)^{1/2} \sim t\left(\frac{\rho_\perp}{\bar{\rho}}\right)^{\nu}, \tag{12}$$

with $\nu = 1 + \frac{\ln(1+\rho_\parallel^2/\rho_\perp^2)}{2\ln(\rho_\perp/\bar{\rho})}$. It follows that we have $\frac{1}{2} \lesssim \nu \lesssim 1$ for $\rho_\parallel$ ranging from $\rho_\parallel = \rho_\perp$ to $\rho_\parallel = 0$. This relation holds for the random walk of a free particle. This is generally not true for our case in which an adatom cannot continue to "walk" after it becomes part of a cluster. The real situation is that some atoms form clusters as they deposit on the surface, and others diffuse for a significantly long time. Since we are considering an average effect, Eq. (12) should be replaced by an ensemble average. As a result, we have

$$\tau = t\left(\frac{\langle\rho_\perp\rangle}{\bar{\rho}}\right)^{\nu} = t\left(\frac{\rho_\perp}{\bar{\rho}}\right)^{z} \sim td_c^{-z}. \tag{13}$$

Since $\rho_\perp > \langle\rho_\perp\rangle$, we have $z < \nu$. The average effect quantitatively reduces and sets an upper bound to the value of z, and we finally have $\frac{1}{2} \lesssim z < 1$. From simulations (see Fig. 6), we find that the upper bound is about 0.75, which is consistent with experimental results for $I_h = 0$ and small I_h (see Table I). For large I_h, clusters continue to diffuse and the upper bound is close to 1. Consequently, the formations of clusters generally perturb the behaviors of a random walk, but characteristic features of the two-dimensional random walk model can still provide a consistent picture for surface diffusion in the cluster formation of adatoms on CNTs.

VI. DISCUSSION

In conclusion, we have investigated the curvature effect on the surface diffusion of Ag adatoms on CNTs. We first set up an experiment for depositing Ag atoms on CNTs to observe the behaviors of the cluster formation of Ag adatoms. The flux of Ag atoms was kept constant in the experiment to exclude the existence of the finite-size effect. Based on the analysis of the cluster density as a function of the deposition time for different diameters of CNTs, the scaling form of Eq. (7) was derived to describe the curvature effect on surface diffusion in the first-order approximation. By using the numerical simulations, the scaling form is further verified to be true. Consequently, we conclude that the curvature effect on surface diffusion can be described by the relation between the deposition time t and the scaled deposition time τ in the form of $\tau \sim td_c^{-z}$ with the exponent z for characterizing geometric properties of CNTs and the nanotube helicity. The value of z is determined from empirical data and it ranges from 0.5 to 0.75 for the case of $I_h = 0$ in this work. For the case $I_h \neq 0$, the value of z determined from the scaling form is essentially overestimated for large I_h's and it ranges from 0.5 to 1.0. The scaling form and the value of the exponent z can be explained from the consideration of the anisotropic two-dimensional random walk model.

In our simulation, the square lattice has been used for simplicity, instead of using the triangular or honeycomb lattice which is closer to a real situation. It is considered that simulations on triangular and honeycomb lattices may provide improvements in the demonstration, but the final conclusion does not change since the diffusion rate $\vec{\rho}$ has been generalized as two components in our simplified version. The present work mainly provides a simple exploration on the curvature effect on surface diffusion, a thorough investigation based on more realistic lattices will be reported elsewhere.

The CNTs used in our study are multiwall CNTs, but we expect the experiment and analysis can also be performed on single-wall CNTs. It follows that the current work also inspires further studies on the detection of the nanotube helicity. For example, depending on its helicity, the single-wall CNT can be either metallic or semiconducting. However, the armchair-type single-wall CNT is always metallic. Since the analysis of the curvature effect in this work implies stronger dependence of curvature effect for the armchair-type CNT from the value of z, it will be useful to develop a practical scheme to test the prediction our work offers. We are working in this direction and will report the further results in a future paper.

ACKNOWLEDGMENTS

This work was supported by the National Science Council of the Republic of China (Taiwan) under Grant No. NSC 94-2112-M-001-014 and NSC 95-2119-M-002-001(M.-C.W., C.-L.L., C.-K.H.) and NSC 94-2120-M-001-006 (H.-C.C., Y.-H.L., L.-W.H., C.-S.C., T.-T.T., T.H.). C.-L.L. was also supported by the National Natural Science Foundation of China under Grant No. 10574088.

*Electronic address: mcwu@phys.sinica.edu.tw
†Electronic address: huck@phys.sinica.edu.tw
‡Electronic address: jasonc@sinica.edu.tw

[1] M. C. Bartelt and J. W. Evans, Phys. Rev. B **46**, 12675 (1992).
[2] F. Besenbacher, Rep. Prog. Phys. **59**, 1737 (1996).
[3] T.-T. Tsong, Physica A **357**, 250 (2005).
[4] S. Iijima, Nature (London) **354**, 56 (1991).
[5] Y. Zhang and H. Dai, Appl. Phys. Lett. **77**, 3015 (2000); Y. Zhang, N. W. Franklin, R. J. Chen, and H. Dai, Chem. Phys. Lett. **331**, 35 (2000).
[6] D. J. Shu and X. G. Gong, J. Chem. Phys. **114**, 10922 (2001).
[7] A. V. Krasheninnikov, K. Nordlund, P. O. Lehtinen, A. S. Foster, A. Ayuela, and R. M. Nieminen, Phys. Rev. B **69**, 073402 (2004).
[8] More accurately, the surface area is an area focused by the TEM. It is a portion of the cylindrical surface of a CNT. The length l

here is thus the length of the segment located in the field of microscope.

[9] E. Durgun, S. Dag, V. M. K. Bagci, O. Gülseren, T. Yildirim, and S. Ciraci, Phys. Rev. B **67**, 201401(R) (2003).

[10] There are two ways to derive the relation between $\Delta\rho$ and I_h. From considering the relation between the jumping frequency Γ at temperature T, $\Gamma=\Gamma_0 \exp(-E_d/kT)$, where Γ_0 is the frequency of small oscillation of the adatom in the potential well or the attempt frequency, E_d is the activation barrier height, and k is the Boltzmann constant, we have $\Delta\rho \propto T$, and thus $\Delta\rho \propto I_h$ in our system. Furthermore, for a highly efficient heating system, the function form can be estimated from the relation between energy and momentum, thermal energy $\sim I_h^2 \sim \Delta(mv^2) \sim (\Delta\rho)^2$, where m and v are the adatom mass and velocity. Consequently, we have the same linear relation, $\Delta\rho \propto I_h$.

[11] C.-K. Hu, Phys. Rev. B **29**, 5103 (1984); **29**, 5109 (1984); **46**, 6592 (1992).

[12] A. E. Ferdinand and M. E. Fisher, Phys. Rev. **185**, 832 (1969).

[13] F. G. Wang and C.-K. Hu, Phys. Rev. E **56**, 2310 (1997).

[14] Y. Okabe *et al.*, Phys. Rev. E **59**, 1585 (1999); Y. Tomita, Y. Okabe, and C.-K. Hu, Phys. Rev. E **60**, 2716 (1999); C.-K. Hu, J.-A. Chen, and C.-Y. Lin, Physica A **266**, 27 (1999); M.-C. Wu, C.-K. Hu, and N. Sh. Izmailian, Phys. Rev. E **67**, 065103(R) (2003); N. Sh. Izmailian, K. B Oganesyan, M.-C. Wu, and C.-K. Hu, Phys. Rev. E **73**, 016128 (2006); M.-C. Wu, Phys. Rev. E **73**, 046135 (2006).

[15] C.-K. Hu, C.-Y. Lin, and J.-A. Chen, Phys. Rev. Lett. **75**, 193 (1995); **75**, 2786(E) (1995); Physica A **221**, 80 (1995); C.-K. Hu and C.-Y. Lin, Phys. Rev. Lett. **77**, 8 (1996); C.-K. Hu and F.-G. Wang, J. Korean Phys. Soc. **31**, S271 (1997); H.-P. Hsu, S. C. Lin, and C.-K. Hu, Phys. Rev. E **64**, 016127 (2001); H. Watanabe, S. Yukawa, N. Ito, and C.-K. Hu, Phys. Rev. Lett. **93**, 190601 (2004); H. Watanabe and C.-K. Hu, Phys. Rev. Lett. **95**, 258902 (2005).

[16] A similar definition of scaled time for a lattice dynamic system can be found in P. M. Gade and C.-K. Hu, Phys. Rev. E **73**, 036212 (2006).

[17] There have been studies of the cluster growth of Ag on planar surface, see e.g., J. M. Zuo and B. Q. Li, Phys. Rev. Lett. **88**, 255502 (2002). There is no report of the favorable binding sites of Ag atom.

[18] F. Family and P. Meakin, Phys. Rev. Lett. **61**, 428 (1988).

[19] W. H. McCrea and F. J. W. Whipple, Proc. R. Soc. Edinburgh **60**, 281 (1940).

[20] E. W. Weisstein, *Random Walk—2-Dimensional*, from *MathWorld*—A Wolfram Web Resource, http://mathworld.wolfram.com/ RandomWalk2-Dimensional.html